Effects of Sediment Delivery Changes on Carbon Burial Within the Modern and Abandoned Delta Lobes of the Yellow River, China

Jill M. Arriola[1] · Xuchen Wang[2] · Jaye E. Cable[1,3]

Received: 31 August 2018 / Revised: 6 March 2019 / Accepted: 11 April 2019 / Published online: 29 May 2019

Abstract

Globally, deltaic wetlands sequester large volumes of terrestrial and marine-derived organic carbon. Diminishing sediment supply via river diversions, dams, and/or sea level rise threatens this stored carbon by enhancing erosion, thereby potentially releasing CO_2 back to the atmosphere during remineralization of organic matter. The Yellow River delta, located in the Bohai Sea, China, has undergone intense anthropogenic manipulation since the 1950s including rerouting of the river mouth to expand the delta for oil exploitation. The goal of this study is to identify the impacts of river course diversions on sources and rates of carbon burial in the modern and abandoned delta lobes of the Yellow River delta. In 2016, we collected four cores total in abandoned and modern deltaic lobes and measured vertical accretion, total carbon, total nitrogen, $\delta^{13}C$, and *n*-alkanes. The highest average mass accretion rate of 12,470.1 g m^{-2} $year^{-1}$ is observed in the abandoned delta, although it no longer receives direct river sediment input. The modern and abandoned deltas are currently outpacing sea level rise, but vertical accretion rates are influenced by sediment trapping practices in the modern delta and redistribution of eroded sediments in the abandoned. Average carbon burial rates across both delta sites vary between 7.2 and 14.9 g OC m^{-2} $year^{-1}$. Sediment-associated carbon at both sites is dominantly sourced from the Loess Plateau. To conserve wetlands across the Yellow River delta, sediment management practices that periodically reintroduce sediment-laden river water to former river courses, such as in the Mississippi delta, are suggested.

Keywords Carbon burial · Delta · Coastal wetland · River diversion

Introduction

Coastal wetlands, including deltas, provide numerous ecosystem services including nurseries for economically viable fisheries, dampening storm surge and wave energy, and the ability to bury biomass as carbon storage. Deltaic wetlands sequester atmospheric carbon dioxide (CO_2) via large volumes of terrestrial and marine-derived organic carbon (C), approximately 0.07 Gt C $year^{-1}$ globally (Schlünz and Schneider 2000). The amounts of available space and sediment supplied to deltaic wetlands control their seaward expansion and provide elevation for vegetation, such as *Phragmites australis* or *Spartina alterniflora*, to proliferate (Kirwan and Megonigal 2013). However, previously prograding river delta lobes and their associated wetlands are prone to subsidence and erosion in the absence of river sediment deposition, such as when a river avulsion occurs (Day et al. 2000; Blum and Roberts 2009; Ye et al. 2015). Human influences, including climate change, such as deltaic diversions, river dams, and sea level rise (SLR), also change the growth rate of delta lobes and may result in the sequestered C within these wetlands becoming vulnerable to remineralization processes.

Alterations of global river courses and decreasing sediment concentrations are widely recognized to have impacted lateral deltaic sustainability, such as at the mouths of the Mississippi and Yellow (Huanghe) rivers (Day et al. 2016a). Two apparent consequences of levee construction along the Mississippi River are the reduced runoff of water and eroded sediments from floodplains to feed the river system and the reduction in delivery of water and sediments to wetlands downstream. This

Communicated by Rui Santos

✉ Jill M. Arriola
arriola@email.unc.edu

[1] Department of Marine Sciences, University of North Carolina at Chapel Hill, Chapel Hill, NC 27599, USA

[2] Key Laboratory of Marine Chemistry Theory and Technology, Ocean University of China, Qingdao 266003, China

[3] Environment, Ecology, and Energy Program, University of North Carolina at Chapel Hill, Chapel Hill, NC 27599, USA

hardening and channelization of the Mississippi for the past 300 years has deprived the surrounding deltaic wetlands of the vital sediment deposition needed to counteract subsidence and SLR which has resulted in approximately 4800 km^2 of Mississippi deltaic wetlands lost in the twentieth century (Day et al. 2016b). Similar to the Mississippi River, the rate and location of sediment deposition in the Yellow River (YR) delta have been greatly altered by anthropogenic influences, but beginning in 1128 AD, or 590 years longer than the Mississippi alterations (Yu 2002).

The YR was first diverted to its present location in the southwest shore of the Bohai Sea in 1855 (Wang et al. 2010). Since 1950, the mouth of the river where sediment is discharged into the YR delta has been re-directed four times by human intervention: the Shenxiankou course in 1953, the Diaokou course to the north in 1964, the Qingshuigou river course to the southeast in 1976, and the Qing 8 course in 1996 (Xu 2008; Kong et al. 2015). The constructed diversions of the YR from the north of the delta to the southeast in 1976 and slightly to the northeast in 1996 were performed to facilitate the development of offshore to onshore oil drilling (Kong et al. 2015). Re-directing the sediment supply from the northern Diaokou delta lobe resulted in the northern-most wetland area of the YR delta to laterally retreat 7 km by the year 2000 (Chu et al. 2006).

Controls on sediment delivered to the YR delta include reservoir retention of sediments, changes in precipitation, water consumption, and erosion conservation practices within the YR watershed (Wang et al. 2007). The YR was formerly the second largest river in the world in terms of sediment load with an annual delivery of 1.1×10^9 tons (Zhou et al. 2015). Wang et al. (2007) examined historic sediment discharge trends of the YR and found that 30% of the reduction in sediment load is due to dam creation and subsequent sediment retention. By 2005, the two largest dams below the Loess Plateau, the Sanmenxia and Xiaolangdi, were estimated to retain 11.9 Gt of sediments (Wang et al. 2007).

In an effort to counteract the effects of dam sediment retention and the resulting decrease in sediment delivered to the modern YR delta, the Yellow River Conservancy Commission (YRCC) initiated the Water-Sediment Regulation Scheme (WSRS) in the year 2002. The WSRS releases sediment-laden bottom waters from the Xiaolangdi reservoir once a year in late June/early July which flood and scour coarse sediment from the lower reach river bed (Wang et al. 2007). This annual sediment scouring has resulted in the height of the YR channel in the lower reach to decrease by 1.5 m since 2002 and now delivers approximately half of the annual sediment discharge to the modern delta (Bi et al. 2014).

To understand deltaic wetland stability over time and how changes in river sediment management strategies impact vertical accretion and C burial, studies must include comparisons between historic and newly established deltaic wetlands in high deposition river systems. Recent C burial studies in the YR delta have focused on storage within the wetlands along the modern Qing 8 river diversion (Bai et al. 2012) and C burial between the YR delta and Liaohe delta in the northeastern Bohai Sea (Ye et al. 2015). However, critical C studies are lacking in the deltaic wetlands surrounding the abandoned Diaokou course to understand how long-term C burial in this delta lobe is impacted by alterations in sediment delivery. The abandoned Diaokou course also serves as a proxy for wetlands more vulnerable to SLR in the face of reduced sediment supply and intense land use change. The objectives of this study are (1) to compare the vertical accretion rates and quantity of the buried C within the Diaokou (abandoned) and Qing 8 (modern) course wetlands in the YR delta utilizing TOC and total ^{210}Pb measurements, (2) to identify the sources of C buried at both sites and determine if sources changed congruently with river course alterations via $\delta^{13}C$ and *n*-alkanes, and (3) to identify the primary drivers of C burial variability in the YR delta.

Methods

Study Site and Sample Collection

The Yellow River (YR), known as "the cradle of Chinese civilization," has historically been recognized for the high suspended sediment load which inspired its name (An et al. 2007). Originating high in the Bayan Har Mountains at an elevation of 4600 m, the YR travels 5464 km through a watershed which encompasses 752,440 km^2 of mountains, plateaus, plains, and urban centers to reach the coast (Fig. 1a, b; Bi et al. 2014, Xue et al. 2017). Approximately 90% of the suspended sediment reaching the Bohai Sea from the YR comes from erosion of the fine-grained sandy loam of the Loess Plateau (Wang et al. 2010; Yu et al. 2014). Along its route the river encounters 24 dams and 3147 reservoirs which collect coarse-grained sediments that would otherwise be transported to the coast, thereby allowing fine-grained sediments to accumulate in the delta (Wang et al. 2007).

The YR delta encompasses an area of more than 5000 km^2 and creates an average of 20 km^2 in new land every year (Bi et al. 2014). Average yearly precipitation in the delta ranges from 530 to 630 mm with the highest rainfall occurring during the summer monsoon (Bai et al. 2012), but the annual average evaporation is 1962 mm (Ye et al. 2015). The tidal range along the coast of the delta is < 2 m, but the tidal period varies between diurnal and mixed semi-diurnal depending on location because of an M2 tide amphidromic point located offshore of the former Shenxiangou lobe (Chu et al. 2006). The rate of relative SLR in the Bohai Sea along the YR delta is 4 mm $year^{-1}$ (Bi et al. 2014).

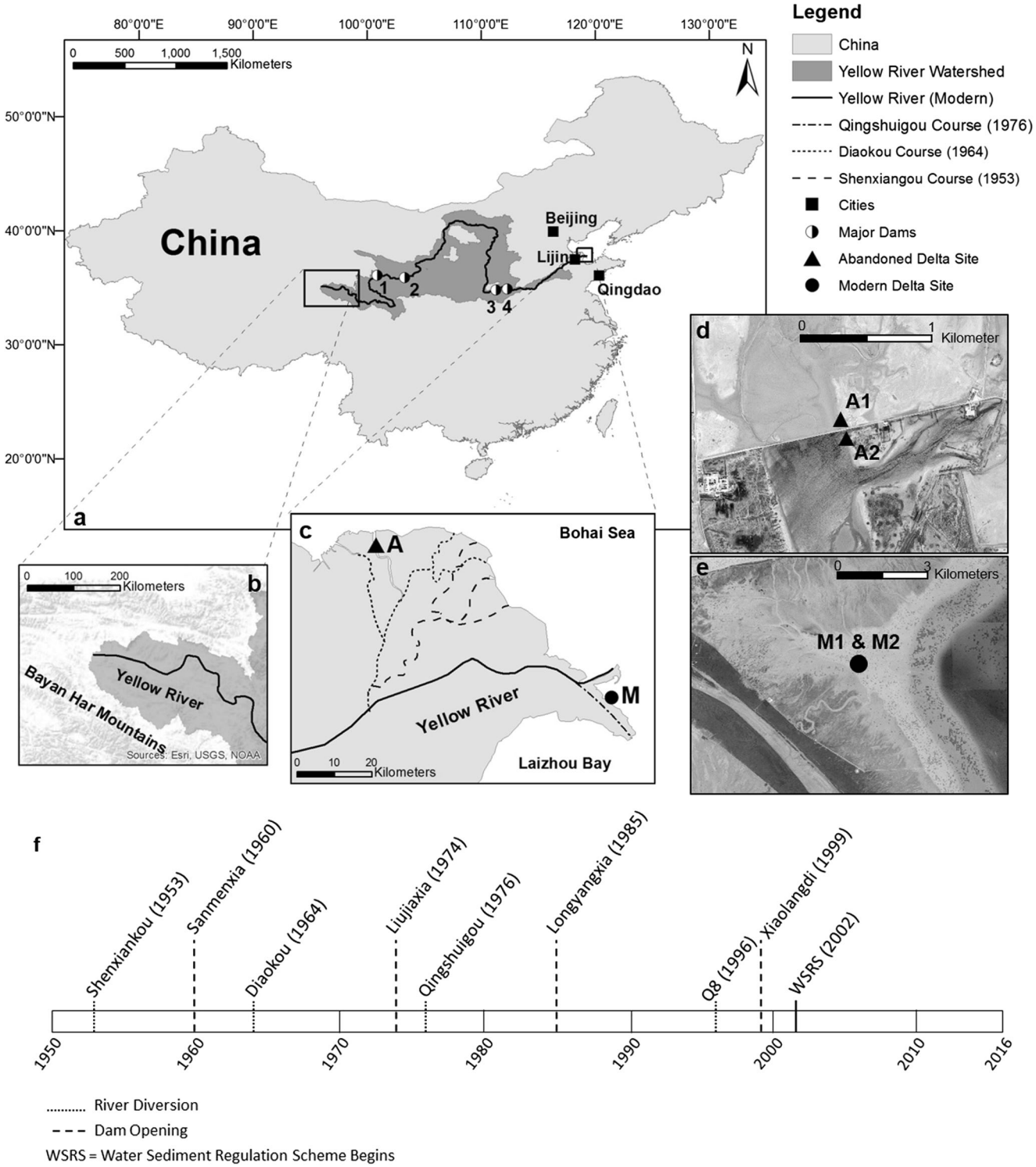

Fig. 1 **a** Map of China showing the Yellow River, the Yellow River watershed, the cities of Beijing, Lijin, and Qingdao, and the locations of the Longyangxia (1), Liujiaxia (2), Sanmenxia (3), and Xiaolangdi (4) dams. **b** Headwaters of the Yellow River in the Bayan Har mountains. **c** A close-up map of the delta which shows the locations of the Shenxiangou, Diaokou, Qingshuigou, and modern river course diversions. The closed triangle indicates the abandoned river course sample site (A) and the closed circle shows the modern river course sample site (M). (Adapted from Xu 2008). **d** Google Earth® image of the abandoned river course site and stations A1 and A2. The elevated road which lies between the two sites clearly demarcates the different hydrologic influences at this site. **e** Google Earth® image of the modern river delta site and stations M1 and M2. **f** Timeline indicating the year of new river diversions (dotted lines), dam openings (dashed lines), and the initiation of the Water-Sediment Regulation Scheme (WSRS)

Two sediment cores were retrieved from two sites, the modern Qing 8 delta lobe (M) and the abandoned Diaokou river course (A), totaling four cores for this study (Fig. 1c). All sediments were collected on 21 June 2016 before the yearly WSRS monitored flooding period using a polycarbonate push core (9.5 cm ID × 50 cm L) pushed into the sediment surface. The diameter and beveled edges on the bottom of the push core minimized compaction of the sediments (< 5 cm) which is assumed to be homogenous throughout the core. Qing 8 delta cores (M1 and M2) were collected about 1 m apart next to a vegetated channel island within a distributary south of the main YR channel (Fig. 1d). Cores were 40 cm in length, sectioned into 2-cm intervals, and kept cold until analysis at Ocean University of China in Qingdao (OUC). Land use around the Qing 8 sampling site varied between agriculture fields, oil drilling platforms, and the Yellow River Mouth Eco-Tourism Area. *Phragmites australis* and *Sueda salsa* comprise > 90% of the vegetation in the modern delta.

In the Diaokou abandoned course (A) in the northern delta plain, about 60 km northwest from the Qing 8 course, land use consisted of salt evaporation ponds, wind turbine fields, oil drilling platforms, and the Yiqian'er National Nature Reserve. Core A1 was retrieved within a tidally influenced vegetated channel edge, dry at the time of sampling, about 50 m from the north side of a concrete road that crosses the former river bed (Fig. 1e). The road was built in 1992 based on Google Earth® map dating and is roughly 1.5 m in height from the river bed. Composed of solid concrete, the road acts as a dam and prevents tidally influenced sedimentation from reaching the landward portion of the river course except during extreme events, such as storm surges. Since sediment accumulation and concentrations are expected to be different compared to the seaward side, a second core for this deltaic lobe (A2) was retrieved about 50 m from the landward (southern) side of the road, but beside a vegetated and ponded area. Vegetation was dominantly *Phragmites australis* with some *Sueda salsa* along the water and channel edge on both sides of the road. Core lengths for A1 and A2 were 30 and 40 cm, respectively. Cores were sectioned into 2-cm intervals and kept cold until analysis at OUC.

Porosity and Percent Organic Matter

Each 2-cm sediment interval was weighed wet, then dried at 60 °C for up to 72 h, and weighed again to determine dry bulk density (Dingman 2002). To calculate porosity (Φ), the volume of the void space, which is assumed to be filled with water with a density of 1.024 g cm^{-3}, was divided by the total volume of the sample interval (Dingman 1984; Breitzke 2006). Half of each dried section was crushed with a mortar and pestle and sieved through a 100-μm mesh. Between 1.5 and 3.0 g of sieved sediment was allocated into pre-weighed glass vials, heated to 150 °C for 1 h to eliminate all sediment-associated water, weighed, and then heated to 550 °C in a muffle furnace for 4 h to obtain percent organic matter (OM).

Carbon and Nitrogen

Sub-samples of sieved sediments for carbon, nitrogen, and stable isotope analyses were combined into 4-cm intervals below 12 cm depth for the modern delta site and station A2. Station A1 samples were combined into 4-cm intervals below 2 cm depth. A separate aliquot of about 1 g of the combined material was acidified with 10% hydrochloric acid overnight to remove any carbonate, rinsed three times with ultrapure water, and dried at 60 °C for 24 h. Sedimentary total organic carbon (TOC) and total nitrogen (TN) were measured using a Thermo Flash 2000 Elemental Analyzer with an analytical precision for the measured values of ± 3% for TOC and ± 4% for TN (e.g., ± 0.03 for TOC).

Stable carbon isotope ($\delta^{13}C$) compositions from A1 and M1 sample intervals, about 15 mg of sediment from each interval, were determined using a Thermo Fisher Delta V Isotope Ratio Mass Spectrometer (IRMS) under continuous flow mode. Values of $\delta^{13}C$ are reported in ‰ relative to the VPDB standard with an analytical precision of less than 0.2‰ ($n = 6$). Terrestrial OM (sourced from C3 photosynthetic pathways) $\delta^{13}C$ isotopes tend to be more depleted than marine sourced OM (Craig 1953). Identifying sources of OM in sediments via $\delta^{13}C$ isotopes combined with the distribution of *n*-alkanes can act as a verification of what processes are driving accretion at the modern and abandoned delta sites, such as carbon delivered either from the Loess Plateau, therefore indicating dominant river sediment provenance, or from heavy industrial land use around the delta.

n-Alkanes

Terrestrial based *n*-alkanes tend to have longer C chains (C_{25}–C_{35}), whereas marine based *n*-alkanes, such as from phytoplankton, are typically shorter (< C_{22}) in length (Wang et al. 2008). Long-chain *n*-alkanes were measured on every other 2-cm sample interval down core as well as intervals that showed changes in sediment physical properties, such as shell hash or iron oxides, which may indicate river course transitions at stations A1, A2, and M1. *n*-Alkanes for station M2 were measured beginning at 18 cm depth and continued down core about every other 2-cm sample interval to investigate local-scale variances in historic *n*-alkane preservation between stations at this site.

Dried and sieved sediment (5.0 g) was extracted using 30–50 mL mixed dichloromethane/methanol (9:1, *v*/*v*) ultrasonically for 10 min three times. 24-Deuterium alkane was added as an internal standard to each sample before the first extraction. The solvent was removed each time after centrifugation at 4800 rpm for 7 min and all extracts were combined. Total

lipid extracts were evaporated to near dryness using a Buchi P-12 multivapor and then re-dissolved in 2 mL hexane and transferred to a small glass vial for further column separation (Wang et al. 2003). *n*-Alkanes were separated using a 1.0 × 20-cm glass chromatography column packed with activated silica gel (100–200 mesh). After adding the extract to the column using a glass pipette, *n*-alkanes were eluted with 25 mL of hexane. The eluate was evaporated down to about 1 mL, then transferred to a glass vial and further concentrated down to 100 μL with high purity N_2. Samples were then stored cold until analyzed for *n*-alkanes (Wang et al. 2003). All glassware used in the sample processing and storage was pre-baked at 550 °C for 5 h.

Composition of long-chain *n*-alkanes ($nC_{14–36}$) were analyzed for all samples using an Agilent 7890B Gas Chromatography (GC). *n*-Alkanes were separated using a Agilent HP-5 capillary column (30 m × 0.32 mm) programmed from 50 to 300 °C at a rate of 3 °C min^{-1} and held at 300 °C for 20 min. Hydrogen was used as the carrier gas with a flow rate set at 1 mL min^{-1}. Individual *n*-alkanes were identified based on the retention time of the authentic standards ($nC_{10–40}$, Sigma), and concentrations of each *n*-alkane homolog were calculated based on the calibration curve of each corresponding standard. The recoveries of the internal standard for all samples determined by GC were all above 80%.

$$\mathrm{ACL} = \Sigma[C_i]i/\Sigma[C_i] \quad (1)$$

$$\mathrm{CPI} = \Sigma \text{ odd } C_{23} \text{ to } C_{33}/\Sigma \text{ even } C_{24} \text{ to } C_{34} \quad (2)$$

The average chain length (ACL) and carbon preference index (CPI) of *n*-alkanes infer where terrestrial OM input is more significant in marine sediments (Wang et al. 2003). The ACL of the alkanes, based on C_{23} to C_{33} chain lengths, found in the sediments identifies which *n*-alkane is dominant at that interval (Eq. 1; Wang et al. 2003). The CPI of *n*-alkanes is useful in identifying sources of OM in marine sediments because higher CPIs are more likely sourced from terrestrial higher plants and not marine organisms, whereas CPIs closer to 1 indicate that the OM has undergone microbial degradation (Johnson and Calder 1973; Wang et al. 2003; Tanner et al. 2010). For this study the chain lengths used to calculate the CPI range from C_{23} to C_{34} (Eq. 2).

^{210}Pb

Total ^{210}Pb activities were measured for each sample interval for all cores and were determined via isotope-dilution alpha spectrometry for the granddaughter isotope, ^{210}Po, which is assumed to be in secular equilibrium with ^{210}Pb. A 1.4- to 1.6-g aliquot of the dried, homogenized sediment was spiked with 1 mL (~ 20 dpm) of ^{209}Po and microwave-digested for 4 h and 20 min up to 95 °C in 15 mL of 15 M nitric acid using a Microwave Accelerated Reaction System (MARS®). Samples were transferred to centrifuge tubes and centrifuged twice at 3500 rpm for 8 min. The supernatant was then transferred to Teflon beakers after each centrifuge and allowed to evaporate on a hot plate (between 85 and 95 °C) until nearly dried. Drops of hydrogen peroxide were added to aid in dissolving any residual organic matter. About 15 mL of deionized water was then added to each evaporated sample and titrated with ammonium hydroxide (between 1 and 5 mL) to promote iron precipitation. The samples were centrifuged three times for 8 min at 3500 rpm and rinsed with deionized water before each cycle, to collect the precipitated iron, which serves as a chelating agent for the radionuclides. After discarding the solvent, the iron precipitate was then dissolved using 3.75 mL of 12 M hydrochloric acid and treated with 50 to 60 mg of ascorbic acid to reduce the iron to the Fe^{2+} ferrous state for the electroplating step. Samples were transferred to individual Teflon beakers containing a magnetic stir bar and a labeled steel disc (planchets) coated with Teflon on one side. Beakers were placed on stir plates at 300 rpm for 20 to 40 h to yield maximum recovery while the Po, as a proxy for Pb, was electroplated onto the steel discs. Planchets were carefully removed, rinsed with deionized water, and allowed to air dry before being placed in a Passivated Implanted Planar Silicon (PIPS®) detector for 24 h to count ^{209}Po and ^{210}Po alpha decays.

Since total ^{210}Pb was analyzed using the alpha method, no data exist for other geochronological tracers, such as ^{137}Cs, which can provide an independent validation for accretion models. Instead, we use the known dates of the river course openings and closings for each site to identify abrupt shifts in accretion rates assumed caused by these events as validation for the models. We assumed that the flux of $^{210}Pb_{ex}$ to the surface was constant, but that the rate of the sediment supply was variable because river sediment is the main source of deposition and is not constant due to anthropogenic activities. Therefore, we used the constant rate of supply (CRS) model (Appleby and Oldfield 1978 and adapted by Sanchez-Cabeza and Ruiz-Fernández 2012) for dating the sediments,

$$A_o = \Sigma \left(^{210}\mathrm{Pb}\right)_i \times d_i \times \rho_i \quad (3)$$

$$A_x = A_o e^{-\lambda t} \quad (4)$$

$$t = \frac{1}{\lambda} \ln \frac{A_o}{A_x} \quad (5)$$

where A_o is the total or initial inventory of ^{210}Pb (Bq m^{-2}). The inventory is derived from the sum of ^{210}Pb activity from the surface to the observed depth interval multiplied by the depth of the interval in cm (d_i), and multiplied by the dry bulk density in g cm^{-3} (ρ_i) of that interval (Eq. 3). A_x is the activity of

^{210}Pb for a given depth interval and λ is the ^{210}Pb decay constant of 0.03114 year^{-1} (Eq. 4; Appleby and Oldfield 1978). Equation 4 is rearranged to solve for the time (t) it took the given sediment to accumulate (Eq. 5). Dividing the depth by t for that interval provides the sediment vertical accretion rate (VAR) in cm year^{-1}. Total sediment mass accumulation rates (MAR; g m^{-2} year^{-1}) were calculated by multiplying the dry bulk density (g cm^{-3}) by the VAR for each interval. Carbon burial rates (CBR; g C m^{-2} year^{-1}) were derived by multiplying the MAR by the TOC concentration (mg C g_{sed}^{-1}) for each interval.

River Discharge Data Collection

Yearly river sediment and water discharge data was obtained from the Lijin Hydrologic Station, located about 100 km upstream from the delta (Fig. 1a), via the Yellow River Sediment Bulletin published by the YRCC for the years 1950 to 2016 (www.yellowriver.gov.cn/nishagonggao).

Results

Mean values of porosity, % OM, TOC, TN, δ^{13}C, VAR, MAR, and CBR for all stations are available in Table 1.

River Sediment Concentrations

Both sediment and water discharge have declined since 1950, but the combined impact on sediment concentration of these decreases are not apparent until the year 2000 (Fig. 2). Since the construction of four major dams in the upper (Liujiaxia in 1974 and Longyangxia in 1985) and lower (Sanmenxia in 1960 and Xiaolangdi in 1999) reaches of the river, the amount of sediment passing through the Lijin hydrologic station has dropped by an order of magnitude to a concentration of 1.3 g L^{-1} in 2016 (Figs. 1 and 2; Wang et al. 2007, Zhou et al. 2015). A clear decrease in sediment concentration occurs after the opening of the Xiaolangdi dam in 1999 from 28.1 to 4.6 g L^{-1} in the year 2000 (Fig. 2).

Sediment Characteristics and Age-Depth Chronology

Porosity ranges between 0.32 and 0.60 for both sites (Fig. 3a). Porosity hovers around 0.50 down core at all stations. Percent OM for both sites ranges between 0 and 0.25% (Fig. 3b). No obvious trends were observed in % OM down core at either site, but % OM is generally highest in the top 10 cm at the M1 station. Dry bulk density (DBD) ranges between 1.15 and 2.34 g cm^{-3} for the modern (M) delta and between 1.31 and 2.23 g cm^{-3} in the abandoned (A) delta (Fig. 3c). Both the lowest and highest DBDs are found in the modern delta.

Concentrations of TOC range between 0.04 and 0.22% dry weight (dw; Fig. 3d). TOC in the modern delta site is around 0.1% dw with depth, but more variation appears in the abandoned delta. The highest TOC is seen at the surface at A2, but then decreases and stays around 0.05% dw with depth. TN concentrations are at least an order of magnitude less than TOC and range between 9.2×10^{-6} and 0.03% dw for both sites (Fig. 3e). TN was below detection for 10 out of 21 samples, mostly at station A2, in the abandoned delta site.

δ^{13}C values of TOC ranges between −22.6 and−26.1‰ and between −22.0 and −24.3‰ for stations M1 and A1, respectively (Fig. 3f). No obvious trend exists down core in regard to δ^{13}C at either station, but the most enriched samples for each station are found at the surface. The most depleted δ^{13}C samples are found at 30 cm depth at M1 and 24 cm depth at A1.

Surface activity of total ^{210}Pb was generally around 13 Bq kg^{-1} at the modern delta site, but was higher at the abandoned delta site where activities were 19 and 39 Bq kg^{-1} at A1 and A2 stations, respectively (Fig. 4). Inventory of ^{210}Pb for stations A1, A2, M1, and M2 are 6573.9 Bq m^{-2}, 13,066.6 Bq m^{-2}, 8463.7 Bq m^{-2}, and 9378.9 Bq m^{-2}, respectively. The inventory of ^{210}Pb for both cores from the modern site are similar to each other, which is expected, but the cores from the abandoned site are different

Table 1 Means (± 1σ) for porosity, percent organic matter (OM), dry bulk density (DBD; g cm^{-3}), total organic carbon (TOC; %), δ^{13}C (‰), vertical accretion rates (VAR; cm year^{-1}), mass accumulation rates (MAR; g m^{-2} year^{-1}), and carbon burial rates (CBR, g OC m^{-2} year^{-1}) for all stations

Station ID	Porosity φ	OM %	DBD (g cm^{-3})	TOC %	δ^{13}C ‰	VAR (cm year^{-1})	MAR (g m^{-2} year^{-1})	CBR (g OC m^{-2} year^{-1})
M1	0.51	0.13	1.96	0.10	−24.2	0.7	10,638.0	14.9
	(0.05)	(0.05)	(0.21)	(0.02)	(1.1)	(0.4)	(6019.8)	(8.2)
M2	0.49	0.13	1.97	0.09	N/A	0.4	10,704.2	7.2
	(0.05)	(0.04)	(0.22)	(0.01)		(0.2)	(6233.4)	(4.0)
A1	0.50	0.12	1.92	0.11	−23.3	0.4	5705.2	8.3
	(0.04)	(0.04)	(0.20)	(0.03)	(0.8)	(0.2)	(2682.0)	(5.8)
A2	0.52	0.12	1.90	0.08	N/A	0.7	12,470.1	11.6
	(0.03)	(0.05)	(0.19)	(0.05)		(0.5)	(7467.7)	(9.4)

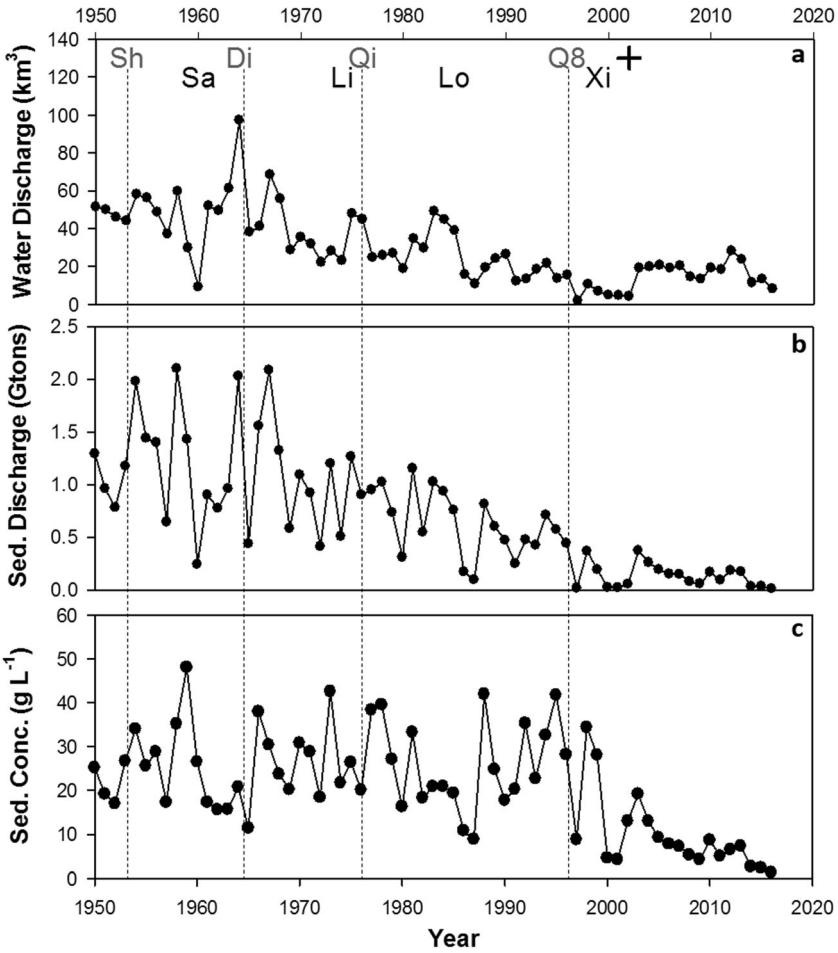

Fig. 2 **a** Water discharge (km^3), **b** sediment discharge (Gt), and **c** sediment concentration (g L^{-1}) through the Lijin Hydrologic Station from 1950 to 2016. Listed in the top portion of graph (**a**) are river diversions in gray with vertical dashed lines (Sh = Shenxiankou (1953), Di = Diaokou (1964), Qi = Qingshuigou (1976), Q8 = Qing 8 (1996)), dam openings in black (Sa = Sanmenxia (1960), Li = Liujiaxia (1974), Lo = Longyangxia (1985), Xi = Xiaolangdi (1999)), and the initiation of the WSRS in 2002 (+)

from the modern site and from one another. A major contributor to the decrease in ^{210}Pb inventory for station A1 is the shorter length of the core which reduces the overall inventory. The higher ^{210}Pb inventory at station A2 is likely influenced by the road that crosses the old river bed which has eliminated the periodic tidal inundation and created a pond on the landward side. This dam creates a more constant water column over station A2 and traps ^{210}Pb transported from the surrounding catchment, both which allow for an increase in ^{210}Pb concentrations, thereby increasing the overall inventory (Appleby 1998).

Vertical accretion rates (VARs) at the sediment surface at stations A1, A2, M1, and M2 are 0.6 cm year^{-1}, 1.3 cm year^{-1}, 1.4 cm year^{-1}, and 0.8 cm year^{-1}, respectively (Fig. 5). Vertical accretion rates generally decrease with depth. Station M1 displays almost consistent VARs between the years 1996 and 2011, whereas station A2 shows a wide range of VARs between 1995 and 2016. Average VARs for the periods of record at stations A1, A2, M1, and M2 are 0.4 cm year^{-1}, 0.7 cm year^{-1}, 0.7 cm year^{-1}, and 0.4 cm year^{-1}, respectively (Table 1). The average VAR for all stations is 0.5 ± 0.4 cm year^{-1}.

Surface mass accretion rates (MARs) for stations A1, A2, M1, and M2 are 10,575.3 g m^{-2} year^{-1}, 17,157.2 g m^{-2} year^{-1}, 19,751.6 g m^{-2} year^{-1}, and 21,580.4 g m^{-2} year^{-1}, respectively (Fig. 5). MARs are typically highest at the surface and decrease with depth except at station A2 where the highest MAR of 26,759.9 g m^{-2} year^{-1} was deposited around 2011 (Fig. 5). Average sediment MARs for A1, A2, M1, and M2 are 5705.2 g m^{-2} year^{-1}, 12,470.1 g m^{-2} year^{-1}, 10,638.0 g m^{-2} year^{-1}, and 10,704.2 g m^{-2} year^{-1}, respectively (Table 1). The average MAR for all stations is 10,157.6 ± 6369.2 g m^{-2} year^{-1}.

Surface carbon burial rates (CBRs) for stations A1, A2, M1, and M2 are 19.1 g OC m^{-2} year^{-1}, 36.8 g OC m^{-2} year^{-1}, 19.9 g OC m^{-2} year^{-1}, and 5.9 g OC m^{-2} year^{-1}, respectively (Fig. 5). CBRs at station M1 appear to be stable near the surface, whereas M2 shows a sharp decrease. Most stations show variability in CBRs after the mid-1990s except station A1. Average CBRs for A1, A2, M1, and M2 are 8.3 g OC m^{-2} year^{-1}, 11.6 g OC m^{-2} year^{-1}, 14.9 g OC m^{-2} year^{-1}, and 7.2 g OC m^{-2} year^{-1}, respectively (Table 1). The average CBR for all stations is 10.7 ± 7.7 g OC m^{-2} year^{-1}.

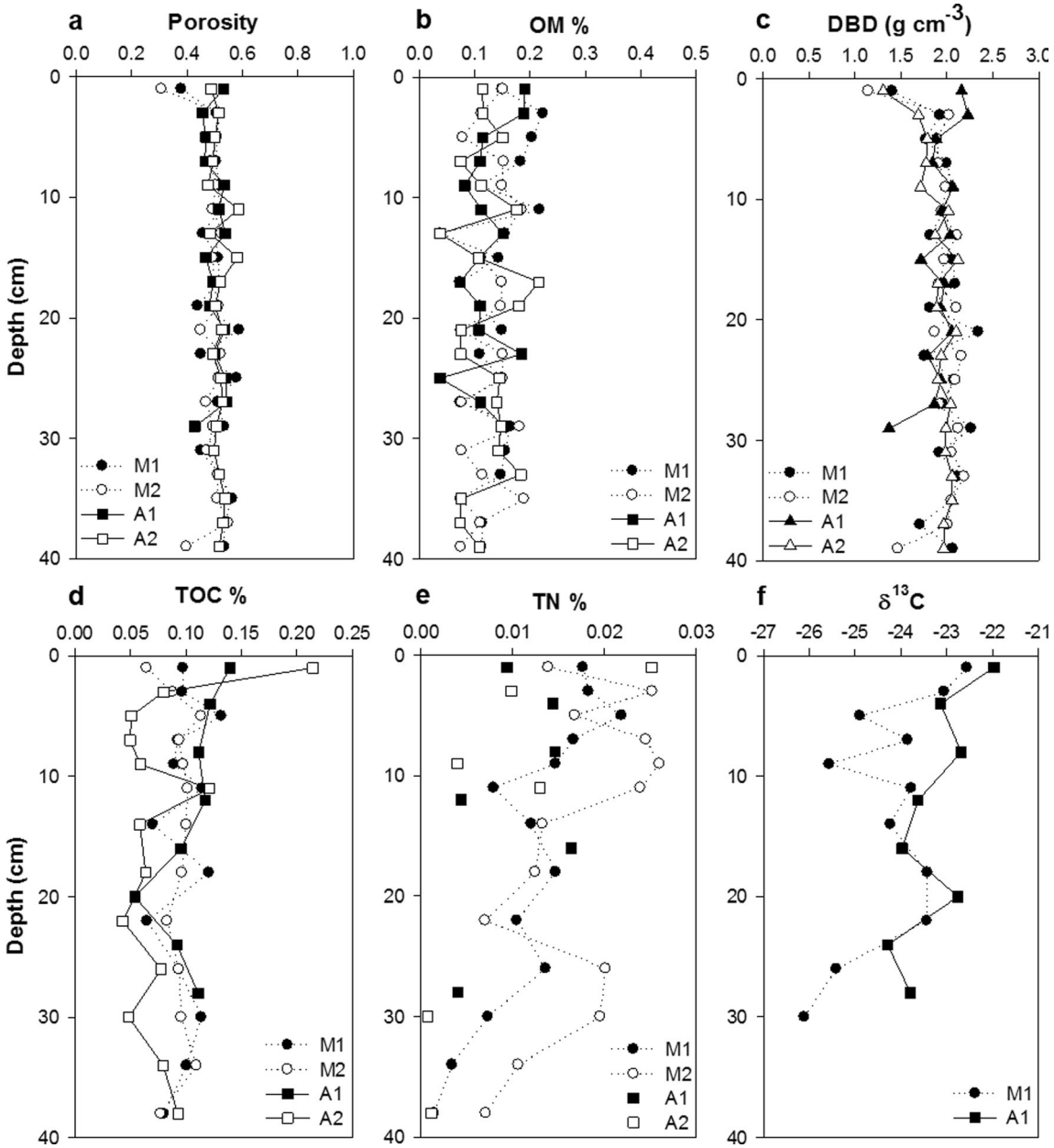

Fig. 3 **a** Porosity, **b** percent organic matter (OM), **c** dry bulk density (DBD; g cm^{-3}), **d** total organic carbon (TOC; %), and **e** total nitrogen (TN; %) for all stations with depth. Lines are not shown for stations A1 and A2 in **e** because about half of the samples were below TN detection limits. **f** $\delta^{13}C$ with depth for stations M1 (closed circle) and A1 (closed triangle). Station M2 is represented by open circles and station A2 is represented by open triangles

The preserved impacts of river diversions and other human disturbances, such as dams and groins, on CBRs ultimately further our understanding of the primary drivers of carbon burial in the YR delta. To identify which variable is dominant, CBRs are plotted versus MARs, TOC concentrations, average VARs, and average DBDs (Fig. 6). The coefficients of determination, or r^2 values, are highest for all stations when CBRs are compared to MARs and VARs, ranging from 0.316 to 0.903 and 0.461 to 0.879, respectively. The weaker correlations between CBRs, TOC, and DBDs and the stronger correlations between VARs and MARs, which are calculated using DBD and VARs, suggest that CBRs are most dependent on VARs.

n-Alkanes

Concentrations of individual *n*-alkanes were detected for chain lengths C_{14} to C_{36} for entire core lengths at stations A1, A2, and M1 (Fig. 7). Concentrations of individual homologs ranged between < 0.1 and 1.3 μg gdw^{-1} at the abandoned site and between < 0.1 and 0.6 μg gdw^{-1} at the modern site. The highest total *n*-alkane concentration in the modern delta,

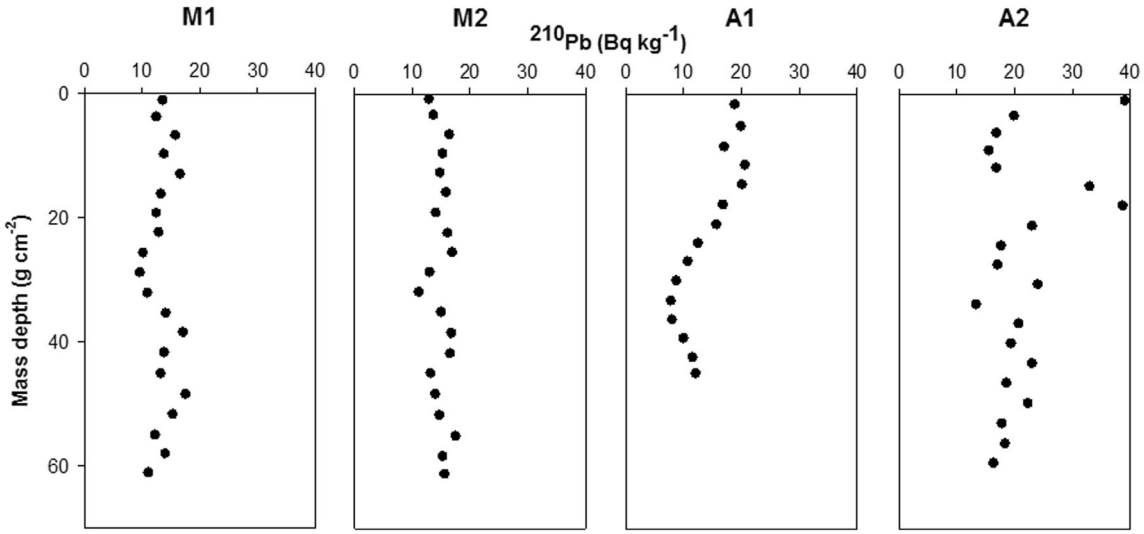

Fig. 4 Total ^{210}Pb (Bq kg^{-1}) versus mass depth (g cm^{-2}) for all stations

3.2 μg gdw^{-1}, was measured at the near surface of station M1 (Table 2). The highest total *n*-alkane concentration in the abandoned site, 8.0 μg gdw^{-1}, was measured at station A2 at a mean depth of 29 cm (Table 2).

In the modern delta, concentrations for the most abundant individual *n*-alkanes for terrestrially sourced OM (C_{27}, C_{29}, C_{31}, C_{33}) are highest at the surface of station M1, but are dominated by C_{29} and C_{31} at around 0.55 μg gdw^{-1}, whereas concentrations of homologs C_{27} and C_{33} are around 0.25 μg gdw^{-1} (Fig. 8). Below the surface for both modern delta stations, concentrations of C_{27}, C_{29}, C_{31}, and C_{33} range between 0.02 and 0.18 μg gdw^{-1}, but C_{29} and C_{33} are usually higher than C_{27} and C_{33}. In the abandoned delta, surface concentrations are also dominated by homologs C_{29} and C_{31} at around 0.3 μg gdw^{-1} and 0.2 μg gdw^{-1} at stations A1 and A2, respectively. Concentrations of homologs at station A1 decrease with depth with all homologs ranging between 0.03 and 0.2 μg gdw^{-1}; again, C_{29} and C_{31} concentrations are higher than C_{27} and C_{33}. The down core trend at station A2 is different than A1 and the modern delta. At a mean depth of 29 cm the concentrations of C_{27}, C_{29}, C_{31}, and C_{33} increase to 0.8, 0.5, 0.3, and 0.1 μg gdw^{-1}, respectively. Concentrations for these four homologs then decrease back to around 0.1 μg gdw^{-1} for the remainder of the core.

The average chain length (ACL) per depth interval ranges between 27.4 and 29.7 in the modern delta site and between 26.4 and 29.5 in the abandoned site (Table 2). The carbon preference index (CPI) was found to range between 1.30 and 5.28 in the modern delta site and between 1.02 and 5.53 in the abandoned delta (Table 2). The lowest CPI values, 1.02 and 1.10, are seen in the abandoned delta station A2 at 21 and 29 cm depth, respectively. The highest CPI values, 5.28 and 5.53, are found at 9 cm depth at station M1 and 25 cm depth at station A1, respectively.

Discussion

Modern Delta Accretion

The balance of sediment supply and erosion has historically been the main driver in the growth and sustainability of the Yellow River delta (YRD), but the direction of delta progradation has been influenced by anthropogenic alternations of river sediment deposition. Utilizing satellite imagery, Bi et al. (2014) observed that from 1996 to 2003, following the latest river diversion, the subaerial delta between the modern Qing 8 delta lobe and the Qingshuigou lobe, experienced an erosional phase at a mean rate of 4.28 km^2 year^{-1}. This erosional phase was caused by the YR experiencing 901 days of no-flow well into the late 1990s where 226 days were in the year 1997 alone (Kong et al. 2015). The erosional phase appears to coincide with a temporary stabilization in the vertical accretion rates (VARs) for both modern delta stations beginning immediately after the opening of the Qing 8 diversion in 1996 and lasting until 2007 and 2001 for stations M1 and M2, respectively (Fig. 5).

Beginning in 2004, satellite imagery revealed the modern delta switched to a lateral accreting phase with a mean lateral growth rate of 6.56 km^2 year^{-1} (Bi et al. 2014). Two groins were constructed around the Qing 8 modern delta lobe after 2005 by the Shengli oil company which extend to the north and south by 1.5 km and 5 km, respectively, to trap suspended sediments that would typically flow into the Bohai Sea, further building the subaerial delta around the active river mouth (Bi et al. 2014). The sediment input from the Qing 8 river diversion combined with the sediment trapped by the groins promote vertical accretion in the modern delta lobe. The shift from an erosion to accretion phase and subsequent lateral growth is confirmed in the VARs results from this study at the modern delta site where station M1 experienced increases

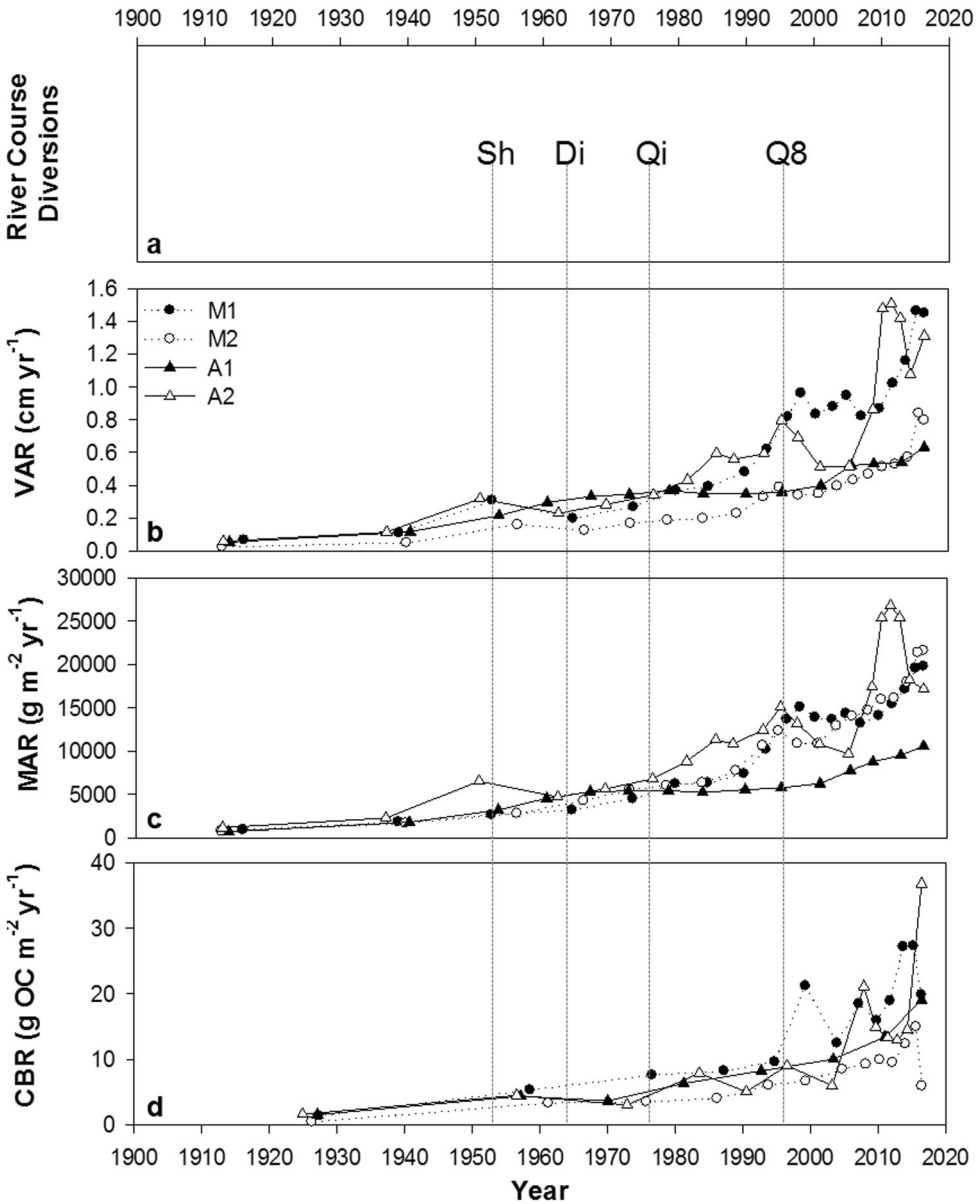

Fig. 5 **a** River course diversions compared to **b** vertical accretion rates (cm year^{-1}), **c** mass accretion rates (g m^{-2} year^{-1}), and **d** carbon burial rates (g OC m^{-2} year^{-1}) for all stations

in VARs post 2004 from 0.9 to 1.4 cm year^{-1} and at station M2 from 0.4 to 0.8 cm year^{-1}.

In a previous study, Ye et al. (2015) used the depth of the Qingshuigou 1976 river diversion paleosol (found between 120 and 300 cm deep) as a time marker to calculate VAR along the YR channel and found vertical accretion rates ranged from 3.9 to 9.7 cm year^{-1} with the highest rate near the mouth (Ye et al. 2015). These rates are substantially higher than our results, but this is likely due to sampling location and the method used for determining accretion rates. The sampling sites used by Ye et al. (2015) are located in established wetlands dominated by *Phragmites* which aid in sediment settlement and accumulation, whereas our study site is located along the edge of a tidal flat south of the YR channel further downstream in the newly established delta. Also, as stated previously, historic sedimentation since the Qingshuigou diversion opening in 1976 has been influenced by periods of erosion and accretion, creating highly variable rates of sedimentation over the past 40 years which are revealed via ^{210}Pb activity.

Wang et al. (2016) examined radioisotope distributions in the intertidal sediments of the modern delta about 500 m from the river channel in 2012. Utilizing ^{137}Cs and ^{210}Pb geochronology, they estimated the average VAR to be about 1.0 cm year^{-1}, with a slight rate increase from 1975 to 1985 of 1.6 cm year^{-1} (Wang et al. 2016). The VARs estimated by Wang et al. (2016) agree with the results of this study which is expected since the sampling locations are both within the intertidal modern deltaic sediments and not established wetlands.

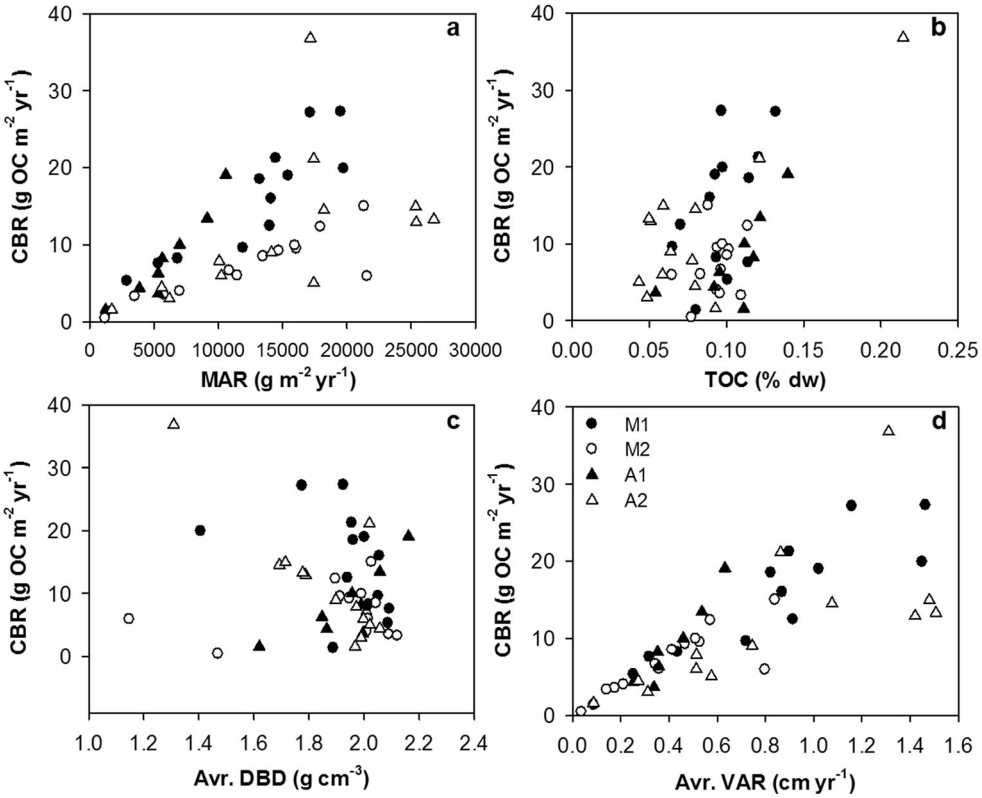

Fig. 6 CBRs versus **a** MAR (g m^{-2} $year^{-1}$), **b** TOC (% dw), **c** average DBD (g cm^{-3}), and **d** average VARs (cm $year^{-1}$) for all stations. Coefficients of determination for the relationship between CBR and VARs show that average VARs are the dominant contributors of CBRs for all stations

Retention of sediment in dams along the YR, in addition to the WSRS implemented by the YRCC, influence not only how much sediment is delivered to the delta but also the grain size of the river sediment load which can impact bulk density and ultimately mass accretion rates (MARs). Median grain size of suspended sediments increased from 18 to 30 μm after 2002 because the WSRS releases sediment-laden bottom waters from the Xiaolangdi reservoir which scours the river bed downstream of the dam (Wang et al. 2010). During the annual WSRS event in 2005, Zhang et al. (2009) measured the dominant sediment grain size passing though Lijin to range between 32 and 63 μm at the beginning of the pulse and was > 63 μm at the end of the 14-day pulse.

Reservoirs and the WSRS are not the only influences of MARs in the modern delta. Increases in MARs after 1980 at the modern delta site appear to be the result of shifting the river course to the Qingshuigou to the southeast in 1976 and to the modern Qing 8 river course in 1996 (Fig. 5). Beginning after 1996, MARs at both M1 and M2 stations briefly stabilized around 13,800 g m^{-2} $year^{-1}$ and 10,800 g m^{-2} $year^{-1}$, respectively, which corresponds with the timing of the erosional phase observed in this location by Bi et al. (2014). After the modern delta began aggrading seaward in 2004, MARs escalated up to a maximum of about 19,750 g m^{-2} $year^{-1}$ and 21,580 g m^{-2} $year^{-1}$ for stations M1 and M2, respectively. The substantial increase in MAR after 2004 suggests that MARs may be influenced by the reintroduction of coarse grain-sized sediment caused by the WSRS starting in 2002. However, YR sediment concentrations passing through Lijin show a decreasing trend since the opening of the Xiaolangdi dam in 1999, opposite of the trend in MARs. These trends reinforce that the trapping of sediments by the groins constructed in 2005, not river sediment concentration, is a primary driver of sediment accumulation in the modern delta.

Abandoned Delta Accretion

Today, no rivers contribute sediment directly to the abandoned Diaokou delta lobe (Chu et al. 2006). Based on satellite imagery, closure of the Diaokou course in 1976 resulted in a loss of 141.3 km^2 of wetlands by the year 2000 (Chu et al. 2006). As illustrated in Fig. 5, VARs for station A1, located on the seaward side of the elevated road, remained relatively stable around 0.4 cm $year^{-1}$ from the 1960s to the early 2000s followed by a gradual increase to the modern VAR of 0.6 cm $year^{-1}$. Although eroded sediments from the northern YR delta are anticipated to be dominantly transported northerly into the Bohai Sea by wave-induced longshore currents (Chu et al. 2006), it is possible that some of the eroded and resuspended sediments are transported and redeposited along the former Diaokou river channel via tides. Tidally delivered and redistributed sediment would explain why station A1 has

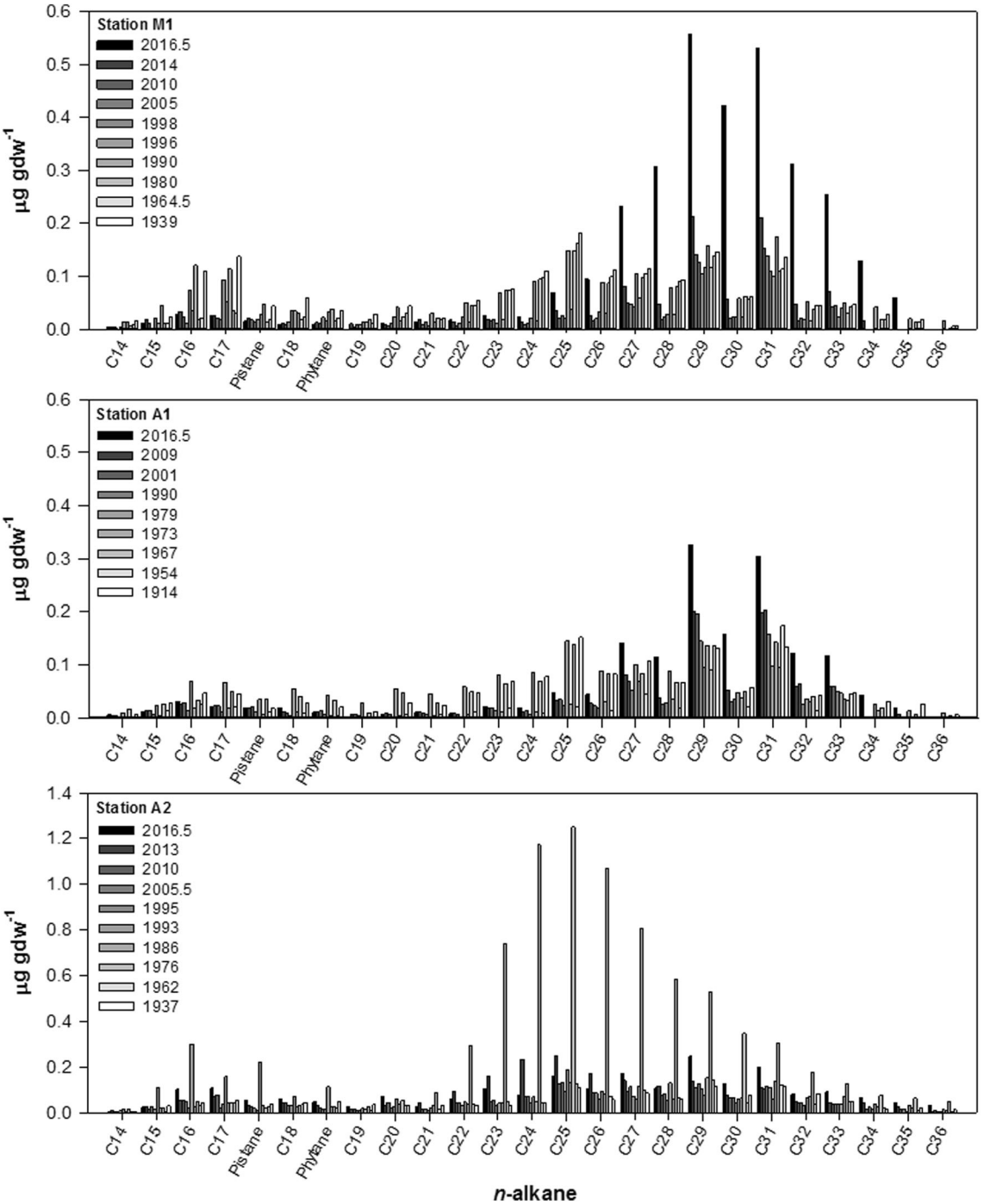

Fig. 7 *n*-Alkane concentrations (µg gdw^{-1}) per year of deposition for stations **a** M1, **b** A1, and **c** A2. Note: Concentration scale for station A2 (**c**) is greater than for stations A1 and M1

continued to vertically accrete even though there is no direct river sediment supply.

The road which crosses the abandoned channel acts as a dam, resulting in water ponding within the abandoned course on the landward side by station A2, and does not appear to directly impact accretion at station A1 on the seaward side. Since 2010, management of the surrounding Yiqian'er reserve has performed freshwater releases in July of each year to prevent erosion, salinization, and habitat degradation of the wetlands (Yang et al. 2017). The initial timing of these freshwater releases correspond with the substantial increase observed in VARs, from 0.9 to 1.5 cm $year^{-1}$, at station A2 (Fig. 5). A large pulse of freshwater likely does erode surficial sediments from the surrounding wetland, leading to sediment focusing in the pond behind the road, thereby increasing VARs at this station.

Table 2 *n*-Alkane year of deposition, carbon preference index (CPI), average chain length (ACL), *n*-alkane concentration in microgram per gram dry weight (μg gdw^{-1}), and *n*-alkane concentrations in milligram per gram of organic carbon (mg g OC^{-1}) for all stations

Sample ID	Year	CPI	ACL	μg gdw^{-1}	mg g OC^{-1}
M1 0–2	2016.5	1.30	29.7	3.2	3.2
M1 4–6	2013.7	3.07	29.4	1.0	0.8
M1 8–10	2009.8	5.28	29.3	0.6	0.7
M1 12–14	2005.0	4.16	29.2	0.6	0.5
M1 18–20	1998.2	2.53	28.8	0.8	0.6
M1 20–22	1996.3	1.41	27.5	1.4	2.1
M1 24–26	1989.9	4.41	29.1	1.1	1.2
M1 28–30	1979.8	1.51	27.4	1.2	1.1
M1 32–34	1964.5	1.56	27.5	1.3	1.3
M1 36–38	1938.8	1.56	27.4	1.8	2.2
M2 18–20	1997.8	1.96	28.0	0.8	0.8
M2 20–22	1995.0	1.69	28.2	0.8	1.0
M2 24–26	1988.7	1.66	28.0	1.1	1.1
M2 28–30	1978.5	1.94	28.4	1.0	1.0
M2 32–34	1966.2	2.10	28.2	1.0	0.9
M2 36–38	1939.9	2.10	28.3	1.1	1.4
A1 0–2	2016.5	1.91	29.5	1.6	1.2
A1 4–6	2009.0	3.17	29.4	0.9	0.8
A1 8–10	2001.2	3.75	29.4	0.9	0.8
A1 12–14	1990.1	3.84	29.4	0.6	0.5
A1 16–18	1978.8	1.53	27.4	1.4	1.5
A1 18–20	1972.9	2.64	29.1	0.7	1.2
A1 20–22	1967.2	1.53	27.4	1.2	2.3
A1 24–26	1953.6	5.53	29.4	0.6	0.7
A1 28–30	1913.7	1.79	27.7	1.3	1.2
A2 0–2	2016.5	1.73	28.1	2.2	1.0
A2 4–6	2012.9	1.22	26.7	2.0	3.9
A2 8–10	2010.3	1.44	27.7	1.2	2.1
A2 12–14	2005.4	1.54	27.7	1.2	2.1
A2 18–20	1995.3	1.84	28.0	0.9	1.4
A2 20–22	1992.8	1.02	27.5	2.1	4.8
A2 24–26	1985.8	1.85	28.3	1.3	1.7
A2 28–30	1976.4	1.10	26.4	8.0	12.6
A2 32–34	1962.4	2.11	28.0	1.1	2.3
A2 36–38	1937.0	1.50	28.4	1.3	1.4

MARs for both abandoned delta stations were around 5000 g m^{-2} $year^{-1}$ after the opening of the Diaokou diversion in 1964 (Fig. 5). Station A1 MARs remain at about 5300 g m^{-2} $year^{-1}$ until 2001 and then begins to increase to the present surface value of around 10,575 g m^{-2} $year^{-1}$. The closing of the Diaokou river diversion in 1976 or road construction in 1992 do not appear to impact historic MARs at station A1. However, after the 1976 river diversion, MARs at station A2 begin to increase, with a maximum MAR of 26,760 g m^{-2} $year^{-1}$ in 2011, which is more than double the MAR at station A1. The MAR maximum at A2 is likely caused by the yearly freshwater flooding by the Yiqian'er reserve management.

In summary, accretion at the modern delta site appears to be influenced not only by river diversions but also by changes in regional climate as well as local sediment trapping by man-made groins. Mass accretion rates seem to be particularly affected by changes in sediment grain size and the Water and Sediment Regulation Scheme which was created to counteract the loss of sediment deposition caused by sediment retention in the dams. Vertical and mass accretion at the abandoned delta have not decreased since the diversion of the Diaokou river course in 1976 as expected, but this may be due to eroded delta sediments being redistributed along the former river channel as well as wetland management practices from the neighboring Yiqian'er Reserve.

Carbon Burial

Source of Organic Material

In 2009, Wang et al. (2012) took monthly samples of YR water passing through the Lijin hydrologic station to examine $\delta^{13}C$ signatures of the terrestrial-sourced dissolved organic carbon (DOC) and particulate organic carbon (POC) and found POC ranged between − 23.4 and − 25.6‰. In another study, Xue et al. (2017) found YR POC $\delta^{13}C$ downstream of Lijin ranged between −22.8 and − 24.1‰. Results from both studies match closely to the $\delta^{13}C$ of this study for M1 and A1 stations, which range between − 22.6 and− 26.1‰ and − 22.0 and − 24.3‰, respectively, which suggests that the OM stored in the abandoned and modern delta is dominantly terrestrial sourced from the YR basin. Furthermore, Xue et al. (2017) utilized a coupled carbon isotopic three end-member mixing model to determine the dominant source of OC inputs to the lower reach of the YR and found that pre-aged soil and fossil OC from weathering accounted for almost 90% of the total POC. In another study, Wang et al. (2012) used ^{14}C to examine the age of YR DOC and POC passing through Lijin and found that POC ranged between 4110 and 8040 years old. These studies, in conjunction with the $\delta^{13}C$ data presented here, suggest that the dominant proportion of OM associated with the Loess Plateau-sourced sediment accumulating in the modern delta is ancient and is preserved within the deltaic sediments.

Deeper sediments at station M1 contain higher concentrations of C_{16} and C_{17} short-chain *n*-alkanes; however, the peaks in C_{16} and C_{17} *n*-alkanes were not observed in the deeper sediments at station M2 (Fig. 7). Burial of short-chain *n*-alkanes at depth implies that the OM is marine sourced, but this conflicts with $\delta^{13}C$ results. Also, using the calculated years of deposition based on ^{210}Pb geochronology for these intervals, peaks in shorter-chain *n*-alkanes at site M1 occurred around

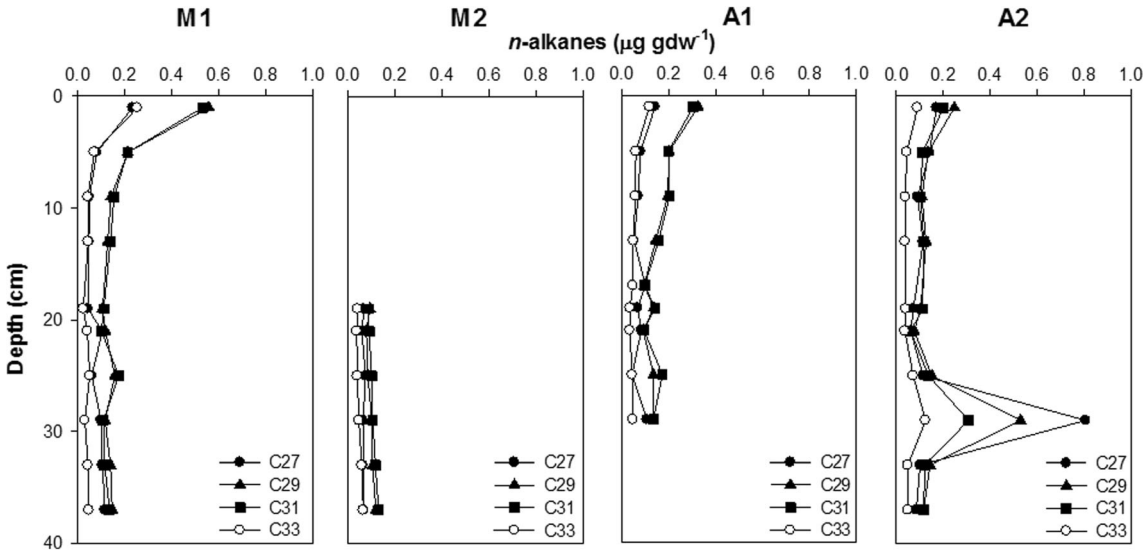

Fig. 8 *n*-Alkanes C_{27}, C_{29}, C_{31}, and C_{33} (μg gdw^{-1}) versus depth (cm) for all stations

1939, 1990, and 1998 (Table 2). The 1990 and 1998 peaks do not correspond exactly with the 1976 Qingshuigou or 1996 Qing 8 river opening diversions, but could represent a lag in response to the new sediment pulse.

The 1964 Diaokou and 1976 Qingshuigou river course diversions in the abandoned delta correspond with peaks in sediment *n*-alkane concentrations at both stations. At station A1, the influence of both river diversions are apparent as slight increases in *n*-alkane concentrations from chain lengths C_{16} to C_{26}. However, the influence of the 1976 Qingshuigou river diversion is more obvious at station A2 and results in the highest total *n*-alkane concentrations, 8.0 μg gdw^{-1}, and the lowest ACL, 26.4, for all stations in this study (Table 2). The 1976 river diversion peak at station A2 is also apparent in *n*-alkane concentrations when comparing the depth distributions of chain lengths C_{27}, C_{28}, C_{31}, and C_{33} across all stations (Fig. 8). In addition, a peak in *n*-alkane concentrations from C_{15} to phytane at station A2 corresponds with the timing of the construction of the elevated road in 1992 (Fig. 7). Higher sediment *n*-alkane concentrations deposited in 1976 and 1992 at station A2, which are not observed at station A1, are likely the result of the redistribution of sediment disturbed by the river diversion and subsequent damming by the road at this location.

The surface of the modern delta site M1 and abandoned station A1 show a strong influence of terrestrially sourced *n*-alkanes with an ACL around 29, whereas the abandoned delta station A2 surface ACL is slightly lower at around 27 (Table 2). CPIs over a value of 3 are generally seen in the upper, but not surface, sediments of stations M1 and abandoned station A1 with the exception of CPI values at an average depth of 25 cm of 4.41 and 5.53, respectively (Table 2). These higher values support the $\delta^{13}C$ results that the OM buried near the surface at stations M1 and A1 are terrestrially sourced. Each station across the YR delta has sediment intervals where the CPI approaches 1, which indicates OM that has been extensively degraded, but these lower values are more dominant at station A2 in the abandoned delta. By combining the influence of intense oil exploitation and water ponding behind the levee next to station A2, it is possible that these *n*-alkanes are dominantly sourced from degraded oil that are washed in from the surrounding area and infiltrate the sediments over time.

Organic Carbon Concentrations

Adjacent oil drilling sites and wetland reserves may contribute to sediment OC concentrations, but these sources are not as influential as the river diversions which distribute the Loess Plateau sediments broadly across the delta. For this study, modern delta sediment-associated TOC ranged between 0.07 and 0.13% dw. During a previous study within the modern delta intertidal sediments just north of the YR channel Wang et al. (2016) found sediment TOC % ranged between 0.21 and 1.2% dw. A study by Bai et al. (2012) determined soil organic carbon (SOC) along two transects within the modern delta, in close proximity to our study site, and found SOC concentrations to range between 0.43 and 4.26 mg OC g_{sed}^{-1}, or 0.043 and 0.426% dw. The modern delta TOC results from the study presented here are lower than the results of Wang et al. (2016), but agree well with Bai et al. (2012).

In another study, Ye et al. (2015) used the frequently utilized TOC and OM relationship from Craft et al. (1991) to quantify carbon burial within established *Phragmites australis* wetlands along the YR channel in the modern delta lobe. Based on their % OM results, Ye et al. (2015) estimated TOC concentrations ranged between 1.5 and 3.6 mg OC g_{sed}^{-1}, or 0.15 and 0.36% dw. Ye et al. (2015)

findings are similar to TOC concentrations directly measured from the modern delta in this study. However, it is important to note that when the % TOC and % OM relationship from our study is plotted against the linear equation derived from Craft et al. (1991), this proxy would underestimate % TOC by an average of twice the measured concentration (Fig. 9).

Since the dominant source of carbon in the modern delta is the river, we compared our results to studies of POC concentrations in the YR. In 2009, Wang et al. (2012) measured the monthly POC concentrations from river water passing through the Lijin hydrologic station and found them to range between 0.37 and 0.79% dw. When comparing the TOC concentration results in the modern delta sediments to the POC coming out of the river, it appears that the intertidal sediments contain about one sixth of the POC concentration in river water. The observed decrease in OC concentrations from riverine POC to OC buried in the YR delta sediments could be attributed to the introduction of the more stable terrestrial-sourced POC to seawater with a higher sulfate concentration, which promotes desorption of OC from mineral particles (Sholkovitz 1976; Jardin et al. 1989), or enhanced remineralization of recalcitrant material in the presence of reactive OM, also known as the priming effect (Guenet et al. 2010; Bianchi 2011).

TOC concentrations in the abandoned delta ranged between 0.04 and 0.21% dw. For comparison, Yang et al. (2017) examined sediment TOC % in the upper 5 cm at sites within intertidal and restored wetland sites within the Yiqian'er reserve just east of the abandoned delta study site well within the established and vegetated wetlands away from the main channel and found the intertidal sediments contained about 5% TOC dw, whereas restored sites contained between 6 and 9% dw. The TOC measurements from Yang et al. (2017) are up to two orders of magnitude higher than our results. This discrepancy is likely due to selection of sampling sites. For our study, stations in the abandoned delta are located along the former river channel and are more influenced by sediments delivered from the river or tides. The increased TOC concentration observed by Yang et al. (2017) is likely enhanced by the accumulation of buried autochthonous OM in the sediments at the wetland sites.

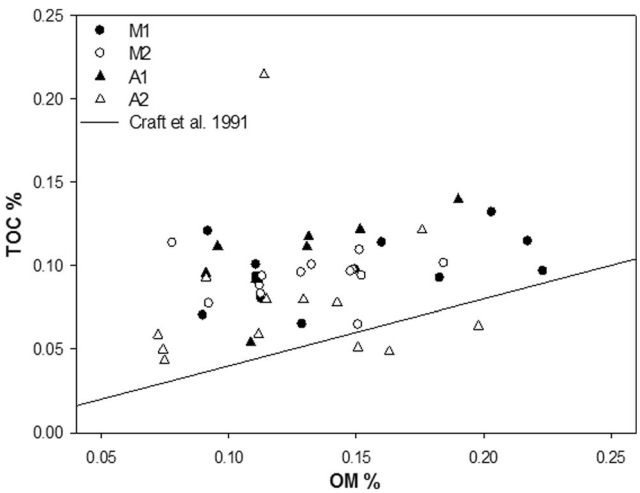

Fig. 9 TOC % versus OM % from this study compared to the linear relationship published by Craft et al. (1991)

Carbon Burial Rates

Although mean CBRs in the modern and abandoned deltas are similar (Table 1), CBRs with depth range between 0.4 and 27.3 g OC m^{-2} $year^{-1}$ and between 1.5 and 36.8 g OC m^{-2} $year^{-1}$, respectively. The average CBR across all sites of 10.7 ± 7.7 g OC m^{-2} $year^{-1}$. For comparison, Ye et al. (2015) found CBRs have a mean of 142 ± 26 g OC m^{-2} $year^{-1}$ along the channel of the YR in the modern delta lobe. Wang et al. (2016) provide TOC and VAR data for the modern YR delta in their study, but CBRs were not calculated. However, by using the average VAR of 1.0 cm $year^{-1}$ and % TOC from Wang et al. (2016) and the average dry bulk density (DBD) from this study, CBRs on the north side of the modern delta river channel are roughly estimated to range between 41.2 and 235.2 g OC m^{-2} $year^{-1}$ with an average of 82.0 ± 33.5 g OC m^{-2} $year^{-1}$. The average carbon burial rate (CBR), based on the averages from this study and the average rates from Ye et al. (2015) and Wang et al. (2016), is 78.6 g OC m^{-2} $year^{-1}$.

Compared to other blue carbon ecosystems, the average CBR of YR deltaic wetlands is about half of the global average CBR for seagrasses (138 ± 38 g OC m^{-2} $year^{-1}$) and about one third of the estimated global CBR average for salt marshes (218 ± 24 g OC m^{-2} $year^{-1}$; McLeod et al. 2011). As for carbon burial rates observed in other deltas, the average CBR in the Liaohe River delta, located about 400 km northeast of the YR delta, is 139 ± 20 g OC m^{-2} $year^{-1}$ (Ye et al. 2015), almost twice the average observed in the YR. When compared to another large depositional river, the Mississippi River delta, Hansen and Nestlerode (2014) found the average CBR for Louisiana salt marshes to range between 145 and 735 g OC m^{-2} $year^{-1}$. These studies suggest that the average CBR observed in the YR delta in this study and across studies, 10.7 g OC m^{-2} $year^{-1}$ and 78.6 g OC m^{-2} $year^{-1}$, respectively, is at least an order of magnitude less than other global deltas.

The YR deltas' ability to keep pace with the rate of relative SLR by vertically accreting sediments determines its vulnerability to inundation and subsequent loss of carbon storage. The Bohai Sea along the YR delta is experiencing SLR rates around 0.4 cm $year^{-1}$ (Bi et al. 2014). With the sediment surface VARs at the abandoned and modern YR delta sites in this study ranging from 0.8 to 1.4 cm $year^{-1}$, the net vertical accretion rates (VAR minus rate of SLR) range from 0.4 to 1.0 cm $year^{-1}$, suggesting that the sediment carbon storage at these sites is not immediately vulnerable to inundation due to

SLR. Although the delta is vertically accreting at both sites at rates faster than relative SLR, shoreline erosion along the former river mouths, such as at the Daiokou site, is already threatening the remaining long-term carbon storage in the historic YR delta.

Without river sedimentation to maintain the extent of the delta, increasing intensity in wave energy due to climate change will enhance the weakening and removal of sediments and their associated carbon from below-ground storage. As of 2013, the area of natural wetlands, which includes intertidal, marsh, and riverine, is 1379.9 km^2 (Zhu et al. 2018). Combined with the average YR delta carbon burial rate of 78.6 g OC m^{-2} $year^{-1}$, the estimated carbon burial for the delta is 0.11×10^{12} g OC $year^{-1}$. Compared to the annual global river delta carbon burial rate of terrestrial OC of 70×10^{12} g OC $year^{-1}$ (Schlünz and Schneider 2000), the Yellow River delta only contributes 0.15% of total delta OC burial. However, the area of natural wetlands has decreased due to erosion and land use change by 1441.5 km^2 since 1973 (Zhu et al. 2018), suggesting that the existing delta wetland carbon storage, although meager, is now at half of its historic capacity.

Impacts of Sediment Management Practices on Delta Sustainability

Increases in vertical accretion rates are shown to dominate carbon burial rates in the YR delta in this study (Fig. 6). These accretion rates appear to coincide with the timing of sediment management strategies, such as river diversions and construction of groins meant to promote land building for economic advantages. However, these management practices are done at the expense of maintaining and conserving existing wetlands in other parts of the delta. Despite no direct river sediment input, the abandoned delta continues to vertically accrete, likely due to resuspended sediments caused by adjacent land use and erosion of the marsh edge. Implications of long-term reduced sediment concentrations and delivery to the abandoned delta are increased lateral delta erosion, decreased wetland stability, and the eventual loss of ancient delta carbon storage.

Offsetting the impacts of reduced sediment discharge from rivers to deltas is a global issue (Syvitski et al. 2009); therefore, many different sediment management strategies are being developed and tested to restore and conserve deltaic wetlands. For example, due to increased subsidence and decreased sediment delivered by the Mississippi River, an anticipated 10,000 to 13,500 km^2 of Louisiana deltaic wetlands will be lost by the year 2100 (Blum and Roberts 2009). As part of the plan to restore these wetlands, Mississippi River water is being reintroduced to the delta through water control structures along the existing river course (Day et al. 2016b). Some of these structures are meant to mimic historic crevasses that occurred along the Mississippi River during floods. Their significance, then as now, is the episodic input of water and sediments to the adjacent wetlands to promote wetland stability (Day et al. 2016c).

In contrast, the current strategy to conserve threatened YR wetlands along the abandoned river course is to pump freshwater onto the wetland surface. While this method supplies nutrients and water to these wetlands, it continues to deprive them of sediment needed to maintain elevation above sea level. We suggest that future sediment management strategies applied to the YR delta focus not only on trapping sediment and building land in the modern delta but these strategies should also include periodically flooding the abandoned river courses with water and sediment from the river. This intermittent flooding strategy could be managed much like a crevasse to enhance sustainability of the entire delta, thereby preserving China's vast carbon storage wetlands. Future research in the YR delta should focus on changes in carbon burial and storage that will occur in the modern delta during and after any future planned river course diversions. Observing wetland carbon storage dynamics before, during, and after the shifting of the river mouth will add to our understanding of future wetland responses associated with river and sediment management strategies.

Acknowledgements We would like to thank Yuanzhi Qi, Yuejun Xue, Tao Zhang, Shen Dan, and Weijing Fu for their assistance in the field and lab, the Key Laboratory of Marine Chemistry Theory and Technology at Ocean University of China in Qingdao for carbon and nitrogen analyses, and J. Paul Liu for the access to the water and sediment discharge data from the Yellow River Sediment Bulletin.

Funding This study was funded by the National Science Foundation East Asia Pacific Summer Institute awarded to JMA (NSF - 1613864).

References

An, S., H. Li, B. Guan, C. Zhou, Z. Wang, Z. Deng, Y. Zhi, Y. Liu, C. Xu, S. Fang, J. Jiang, and H. Li. 2007. China's natural wetlands: past problems, current status, and future challenges. *Ambio* 36 (4): 335–342. https://doi.org/10.1579/0044-7447(2007)36[335:CNWPPC]2.0.CO;2.

Appleby, P.G. 1998. *Dating recent sediments by ^{210}Pb: problems and solutions* (STUK-A–145). Illus, E. (Ed.). Finland.

Appleby, P.G., and F. Oldfield. 1978. The calculation of lead-210 dates assuming a constant rate of supply of unsupported 210Pb to the sediment. *Catena* 5 (1): 1–8. https://doi.org/10.1016/S0341-8162(78)80002-2.

Bai, J., J. Wang, D. Yan, H. Gao, R. Xiao, H. Shao, and Q. Ding. 2012. Spatial and temporal distributions of soil organic carbon and total nitrogen in two wetlands with different flooding frequencies of the Yellow River Delta, China. *Clean - Soil, Air, Water* 40 (10): 1137–1144. https://doi.org/10.1002/clen.201200059.

Bi, N., H. Wang, and Z. Yang. 2014. Recent changes in the erosion–accretion patterns of the active Huanghe (Yellow River) delta lobe

caused by human activities. *Continental Shelf Research* 90: 70–78. https://doi.org/10.1016/j.csr.2014.02.014.

Bianchi, T.S. 2011. The role of terrestrially derived organic carbon in the coastal ocean: a changing paradigm and the priming effect. *Proceedings of the National Academy of Sciences* 108 (49): 19473–19481. https://doi.org/10.1073/pnas.1017982108.

Blum, M.D., and H.H. Roberts. 2009. Drowning of the Mississippi Delta due to insufficient sediment supply and global sea-level rise. *Nature Geoscience* 2 (7): 488–491. https://doi.org/10.1038/ngeo553.

Breitzke, M. 2006. Physical properties of marine sediments. In *Marine Geochemistry*, ed. H.D. Schulz and M. Zabel, 2nd ed., 27–71. Berlin: Springer.

Chu, Z.X., X.G. Sun, S.K. Zhai, and K.H. Xu. 2006. Changing pattern of accretion/erosion of the modern Yellow River (Huanghe) subaerial delta, China: Based on remote sensing images. *Marine Geology* 227 (1): 13–30. https://doi.org/10.1016/j.margeo.2005.11.013.

Craft, C.B., E.D. Seneca, and S.W. Broome. 1991. Loss on ignition and Kjeldahl digestion for estimating organic carbon and total nitrogen in estuarine marsh soils: calibration with dry combustion. *Estuaries* 14 (2): 175–179. https://doi.org/10.2307/1351691.

Craig, H. 1953. The geochemistry of stable isotopes. *Geochimica et Cosmochimica Acta* 3 (2–3): 53–92. https://doi.org/10.1016/0016-7037(53)90001-5.

Day, J.W., L.D. Britsch, S.R. Hawes, G.P. Shaffer, D.J. Reed, and D. Cahoon. 2000. Pattern and process of land loss in the Mississippi Delta: a spatial and temporal analysis of wetland habitat change. *Estuaries* 23 (4): 425–438. https://doi.org/10.2307/1353136.

Day, J.W., J. Agboola, Z. Chen, C. D'Elia, D.L. Forbes, L. Giosan, P. Kemp, C. Kuenzer, R.R. Lane, R. Ramachandran, and J. Syvitski. 2016a. Approaches to defining deltaic sustainability in the 21st century. *Estuarine, Coastal and Shelf Science* 183: 275–291. https://doi.org/10.1016/j.ecss.2016.06.018.

Day, J.W., R.R. Lane, C.F. D'Elia, A.R. Wiegman, J.S. Rutherford, G.P. Shaffer, C.G. Brantley, and G.P. Kemp. 2016b. Large infrequently operated river diversions for Mississippi delta restoration. *Estuarine, Coastal and Shelf Science* 183: 292–303. https://doi.org/10.1016/j.ecss.2016.05.001.

Day, J.W., J.E. Cable, R.R. Lane, and G.P. Kemp. 2016c. Sediment deposition at the Caernarvon crevasse during the great Mississippi flood of 1927: implications for coastal restoration. *Water* 8 (2): 38. https://doi.org/10.3390/w8020038.

Dingman, S.L. 1984. Principles of flow through porous media. In *Fluvial hydrology*, 273–319. New York: W. H. Freeman and Company.

Dingman, S.L. 2002. Water in soils: Infiltration and Redistribution. In *Physical hydrology*, 2nd ed., 220–271. Long Grove: Waveland Press, Inc.

Guenet, B., M. Danger, L. Abbadie, and G. Lacroix. 2010. Priming effect: bridging the gap between terrestrial and aquatic ecology. *Ecology* 91 (10): 2850–2861. https://doi.org/10.1890/09-1968.1.

Hansen, V.D., and J.A. Nestlerode. 2014. Carbon sequestration in wetland soils of the northern Gulf of Mexico coastal region. *Wetlands Ecology and Management* 22 (3): 289–303. https://doi.org/10.1007/s11273-013-9330-6.

Jardin, P.M., N.L. Weber, and J.F. McCarthy. 1989. Mechanisms of dissolved organic carbon adsorption on soil. *Soil Science Society of America Journal* 53 (5): 1378–1385. https://doi.org/10.2136/sssaj1989.03615995005300050013x.

Johnson, R.W., and J.A. Calder. 1973. Early diagenesis of fatty acids and hydrocarbons in a salt marsh environment. *Geochimica et Cosmochimica Acta* 37 (8): 1943–1955. https://doi.org/10.1016/0016-7037(73)90150-6.

Kirwan, M.L., and J.P. Megonigal. 2013. Tidal wetland stability in the face of human impacts and sea-level rise. *Nature* 504 (7478): 53–60. https://doi.org/10.1038/nature12856.

Kong, D., C. Miao, A.G.L. Borthwick, Q. Duan, H. Liu, Q. Sun, A. Ye, Z. Di, and W. Gong. 2015. Evolution of the Yellow River Delta and its relationship with runoff and sediment load from 1983 to 2011. *Journal of Hydrology* 520: 157–167. https://doi.org/10.1016/j.jhydrol.2014.09.038.

McLeod, E., G.L. Chmura, S. Bouillon, R. Salm, M. Björk, C.M. Duarte, C.E. Lovelock, W.H. Schlesinger, and B.R. Silliman. 2011. A blueprint for blue carbon: toward an improved understanding of the role of vegetated coastal habitats in sequestering CO_2. *Frontiers in Ecology and the Environment* 9 (10): 552–560. https://doi.org/10.1890/110004.

Sanchez-Cabeza, J.A., and A.C. Ruiz-Fernández. 2012. 210Pb sediment radiochronology: an integrated formulation and classification of dating models. *Geochimica et Cosmochimica Acta* 82: 183–200. https://doi.org/10.1016/j.gca.2010.12.024.

Schlünz, B., and R.R. Schneider. 2000. Transport of terrestrial organic carbon to the oceans by rivers: re-estimating flux and burial rates. *International Journal of Earth Sciences* 88 (4): 599–606. https://doi.org/10.1007/s005310050290.

Sholkovitz, E.R. 1976. Flocculation of dissolved organic and inorganic matter during the mixing of river water and seawater. *Geochimica et Cosmochimica Acta* 40 (7): 831–845. https://doi.org/10.1016/0016-7037(76)90035-1.

Syvitski, J.P., A.J. Kettner, I. Overeem, E.W.H. Hutton, M.T. Hannon, G.R. Brakenridge, J. Day, C. Vörösmarty, Y. Saito, L. Giosan, and R.J. Nicholls. 2009. Sinking deltas due to human activities. *Nature Geoscience* 2 (10): 681–686. https://doi.org/10.10338/ngeo629.

Tanner, B.R., M.E. Uhle, C.I. Mora, J.T. Kelley, P.J. Schuneman, C.S. Lane, and E.S. Allen. 2010. Comparison of bulk and compound-specific δ13C analyses and determination of carbon sources to salt marsh sediments using n-alkane distributions (Maine, USA). *Estuarine, Coastal and Shelf Science* 86 (2): 283–291. https://doi.org/10.1016/j.ecss.2009.11.023.

Wang, X.C., R.F. Chen, and A. Berry. 2003. Sources and preservation of organic matter in Plum Island salt marsh sediments (MA, USA): long-chain n-alkanes and stable carbon isotope compositions. *Estuarine, Coastal, and Shelf Science* 58 (4): 917–928. https://doi.org/10.1016/j.ecss.2003.07.006.

Wang, H., Z. Yang, Y. Saito, J.P. Liu, X. Sun, and Y. Wang. 2007. Stepwise decreases of the Huanghe (Yellow River) sediment load (1950-2005): impacts of climate change and human activities. *Global and Planetary Change* 57 (3-4): 331–354. https://doi.org/10.1016/j.gloplacha.2007.01.003.

Wang, X.C., M.Y. Sun, and A.C. Li. 2008. Contrasting chemical and isotopic compositions of organic matter in Changjiang (Yangtze River) estuarine and East China Sea shelf sediments. *Journal of Oceanography* 64 (2): 311–321. https://doi.org/10.1007/s10872-008-0025-1.

Wang, H., N. Bi, Y. Saito, Y. Wang, X. Sun, J. Zhang, and Z. Yang. 2010. Recent changes in sediment delivery by the Huanghe (Yellow River) to the sea: causes and environmental implications in its estuary. *Journal of Hydrology* 391 (3-4): 302–313. https://doi.org/10.1016/j.jhydrol.2010.07.030.

Wang, X., H. Ma, R. Li, Z. Song, and J. Wu. 2012. Seasonal fluxes and source variation of organic carbon transported by two major Chinese rivers: the Yellow River and Changjiang (Yangtze) River. *Global Biogeochmical Cycles* 26 (2): 1–10. https://doi.org/10.1029/2011GB004130.

Wang, Q., J. Song, X. Li, H. Yuan, N. Li, and L. Cao. 2016. Environmental evolution records reflected by radionuclides in the sediment of coastal wetlands: a case study in the Yellow River Estuary wetland. *Journal of Environmental Radioactivity* 162-163: 87–96. https://doi.org/10.1016/j.jenvrad.2016.05.015.

Xu, J. 2008. Response of land accretion of the Yellow River delta to global climate change and human activity. *Quaternary International* 186 (1): 4–11. https://doi.org/10.1016/j.quaint.2007.08.032.

Xue, Y., L. Zou, T. Ge, and X. Wang. 2017. Mobilization and export of millennial-aged organic carbon by the Yellow River. *Limnology and Oceanography* 62 (S1): S95–S111. https://doi.org/10.1002/lno.10579.

Yang, W., X. Li, T. Sun, J. Pei, and M. Li. 2017. Macrobenthos functional groups as indicators of ecological restoration in the northern part of China's Yellow River Delta wetlands. *Ecological Indicators* 82: 381–391. https://doi.org/10.1016/j.ecolind.2017.06.057.

Ye, S., E.A. Laws, N. Yuknis, X. Ding, H. Yuan, G. Zhao, J. Wang, X. Yu, S. Pei, and R.D. DeLaune. 2015. Carbon sequestration and soil accretion in coastal wetland communities of the Yellow River Delta and Liaohe Delta, China. *Estuaries and Coasts* 38 (6): 1885–1897. https://doi.org/10.1007/s12237-014-9927-x.

Yu, L. 2002. The Huanghe (Yellow) River: a review of its development, characteristics, and future management issues. *Continental Shelf Research* 22 (3): 389–403. https://doi.org/10.1016/S0278-4343(01)00088-7.

Yu, J., Y. Li, G. Han, D. Zhouw, y. Fu, B. Guan, G. Wang, K. Ning, H. Wu, and J. Wang. 2014. The spatial distribution characteristics of soil salinity in coastal zone of the Yellow River Delta. *Clean - Soil, Air, Water* 42 (3): 311–318. https://doi.org/10.1007/s12665-013-2980-0.

Zhang, L., J. Zhang, and M. Gong. 2009. Size distributions of hydrocarbons in suspended particles from the Yellow River. *Applied Geochemistry* 24 (7): 1168–1174. https://doi.org/10.1016/j.apgeochem.2008.12.033.

Zhou, Y., H.Q. Huang, G.C. Nanson, C. Huang, and G. Liu. 2015. Progradation of the Yellow (Huanghe) River delta in response to the implementation of a basin-scale water regulation program. *Geomorphology* 243: 65–74. https://doi.org/10.1016/j.geomorph.2015.04.023.

Zhu, C., X. Zhang, and Q. Huang. 2018. Four decades of estuarine wetland changes in the Yellow River delta based on Landsat observations between 1973 and 2013. *Water* 10 (7): 933. https://doi.org/10.3390/w10070933.